Water Research 122 (2017) 387–397

Contents lists available at ScienceDirect

Water Research

journal homepage: www.elsevier.com/locate/watres

Equilibria model for pH variations and ion adsorption in capacitive deionization electrodes

Ali Hemmatifar [a], Diego I. Oyarzun [a], James W. Palko [a], Steven A. Hawks [b], Michael Stadermann [b, **], Juan G. Santiago [a, *]

[a] Department of Mechanical Engineering, Stanford University, Stanford, CA, 94305, USA
[b] Lawrence Livermore National Laboratory, 7000 East Avenue, Livermore, CA, 94550, USA

ARTICLE INFO

Article history:
Received 7 April 2017
Received in revised form
16 May 2017
Accepted 17 May 2017
Available online 20 May 2017

Keywords:
Surface functional groups
pH
Activated carbon
Titration
Capacitive deionization
Weak electrolytes

ABSTRACT

Ion adsorption and equilibrium between electrolyte and microstructure of porous electrodes are at the heart of capacitive deionization (CDI) research. Surface functional groups are among the factors which fundamentally affect adsorption characteristics of the material and hence CDI system performance in general. Current CDI-based models for surface charge are mainly based on a fixed (constant) charge density, and do not treat acid-base equilibria of electrode microstructure including so-called micropores. We here expand current models by coupling the modified Donnan (mD) model with weak electrolyte acid-base equilibria theory. In our model, surface charge density can vary based on equilibrium constants (p*K*'s) of individual surface groups as well as micropore and electrolyte pH environments. In this initial paper, we consider this equilibrium in the absence of Faradaic reactions. The model shows the preferential adsorption of cations versus anions to surfaces with respectively acidic or basic surface functional groups. We introduce a new parameter we term "chemical charge efficiency" to quantify efficiency of salt removal due to surface functional groups. We validate our model using well controlled titration experiments for an activated carbon cloth (ACC), and quantify initial and final pH of solution after adding the ACC sample. We also leverage inductively coupled plasma mass spectrometry (ICP-MS) and ion chromatography (IC) to quantify the final background concentrations of individual ionic species. Our results show a very good agreement between experiments and model. The model is extendable to a wide variety of porous electrode systems and CDI systems with applied potential.

1. Introduction

Capacitive deionization (CDI) is a promising technology for reducing water salinity and removing undesirable ionic contaminants from solutions (Porada et al., 2013; Suss et al., 2015). CDI is normally achieved by flowing a salt solution through or near porous carbon electrodes, where an applied bias induces ion migration and salt adsorption within the porous structures (Hemmatifar et al., 2016, 2015; Johnson and Newman, 1971; Kang et al., 2014; Kim and Yoon, 2014; Qu et al., 2016, 2015). Often, the carbon pores are modeled as having a bimodal distribution of so-called macropores and micropores. The solution within macropores is assumed to be net neutral, and macropores are dominantly responsible for transport of ions. Ions are assumed to be stored in the electric double layers within (overlapping) micropores which dominate charge storage (Biesheuvel et al., 2009; Biesheuvel and Bazant, 2010). The nature of micropore adsorption and equilibrium between micropores and macropores is thus at the heart of much of CDI research. An important micropore property that can dramatically impact this coupling is chemical surface charge functionalization (Andelman, 2014; Avraham et al., 2011; Biesheuvel et al., 2015; Cohen et al., 2011; Gao et al., 2017, 2016, 2014). Studies on surface functional groups and the potential or pH at the point of zero charge (PZC) of activated carbon is a long-standing field of study (Babić et al., 1999; Barkauskas and Dervinyte, 2004; Bhatnagar et al., 2013; Corapcioglu and Huang, 1987; Lopez-Ramon et al., 1999; Noh and Schwarz, 1990; Pandolfo and Hollenkamp, 2006). In CDI applications, however, the role of surface functional groups on enhancement of performance has been of

* Corresponding author.
** Corresponding author.
E-mail addresses: stadermann2@llnl.gov (M. Stadermann), juan.santiago@stanford.edu (J.G. Santiago).

http://dx.doi.org/10.1016/j.watres.2017.05.036
0043-1354/

Nomenclature

K_{X_i}	Acid dissociation constant of acidic group X_i (mM)
K_{Y_j}	Acid dissociation constant of basic group Y_j (mM)
$c_{X_i^-}$	Micropore concentration of X_i^- (mM)
c_{X_iH}	Micropore concentration of X_iH (mM)
c_{Y_j}	Micropore concentration of Y_j (mM)
$c_{Y_jH^+}$	Micropore concentration of Y_jH^+ (mM)
$c_{X_i,0}$, $c_{Y_j,0}$	Analytical concentration of i-th acidic and j-th basic group (mM)
$N_{X_i,0}$, $N_{Y_j,0}$	Amount of i-th acidic and j-th basic group (moles)
n_X, n_Y	Number of types of acidic and basic groups
$\sigma_{X_i^-}$, $\sigma_{Y_jH^+}$	Surface charge density of i-th acidic and j-th basic group (C m^{-3})
pK_X, pK_Y	Acid and base pK values
pH_f	Final pH of solution
$pH_{m,f}$	Final micropore pH
pH_{PZC}	pH at the point of zero charge
σ_{chem}	Net chemical charge density (C m^{-3})
σ_{ionic}	Ionic charge density (C m^{-3})
σ_{elec}	Electronic charge density (C m^{-3})
$c_{m,H}$	Micropore concentration of hydronium (mM)
c_H	Concentration of hydronium in the bulk solution (mM)
$c_{m,\pm}$	Micropore concentration of anion or cation (mM)
$c_\pm$	Concentration of anion or cation in the bulk solution (mM)
$z_\pm$	Valence of anion or cation
V_{ext}	External voltage (V)
$\Delta\phi_D$	Donnan potential drop (V)
$\Delta\phi_m$	Micropore potential drop (V)
C_m	Volumetric capacitance of micropores (F m^{-3})
v_m	Micropore volume (m^3)
m_e	Electrode mass (g)
$c_{\pm,0}$	Initial concentration of anion and cation (right after addition of titrant) (mM)
v_{sol}	Final volume of solution (m^3)
v_{sol}^0	Initial volume of solution (m^3)
$v_{titrant}$	Volume of added titrant (m^3)
c_{stock}	Titrant (HCl, NaOH) stock concentration (mM)
$\Gamma_\pm$	Cationic and anionic salt adsorption (moles)
Γ	Net salt adsorption (moles)
Σ_{chem}	Net micropore surface charge (C)
Λ	Charge efficiency
Λ_{chem}	Chemical charge efficiency

significant interest only recently (Gao et al., 2017, 2016, 2015a; Wu et al., 2016).

Current CDI-based models treat chemical surface charge by considering a simple fixed (constant and permanent) charge density (of a certain sign and magnitude in Coulombs per volume) residing within the micropore volume (Biesheuvel et al., 2015). This simple treatment of net surface charge has the effect of modifying the equilibrium charge composition in the micropores. An important implication of surface charge is that the porous material can electrostatically adsorb salt ions from the solution within macropores, sustaining macropore electroneutrality by altering the pH. Notably, this adsorption can occur with no externally applied electric potential. This fixed charge changes the degree of charging of the electric double layers and so fundamentally changes the CDI cell's PZC and the relationship between charge efficiency and applied potential. For example, applied electrical potentials of a sign opposite to the fixed charge first expels ions of charge opposite to the fixed charge before reaching the PZC. Only after crossing the PZC, can electric charges effectively accumulate net charge of the same sign as the fixed charge (Biesheuvel et al., 2015; Gao et al., 2015a, 2015b). Recently, Gao et al. (2015a) and Wu et al. (2016) experimentally demonstrated increases in the charge efficiency, salt-absorption capacity, and operating voltage window of CDI devices with positive surface charge functionalization (treated with ethylenediamine or quaternized poly (4-vinylpyridine)) and negative surface charge (treated with nitric acid) functionalization. While the results presented by Gao et al. (2015a) are in general agreement with a simple fixed-charge amphoteric model for surface charge (Biesheuvel, 2015), a detailed model based on basic physicochemical equilibria which includes pH and an arbitrary composition of acidic and basic surface charge sites within the micropores has yet to be developed.

In this work, we aim to expand upon current models for understanding surface charge effects in porous carbon materials for CDI by coupling the modified Donnan (mD) model (Biesheuvel et al., 2011) with weak electrolyte acid-base equilibria theory (Persat et al., 2009a, 2009b). Namely, we propose a treatment wherein micropores have a certain analytical concentration of acidic and basic groups with their own equilibrium constants (pK). We propose a model wherein the degree of dissociation of (immobile) functional groups within the micropores is governed by their acid dissociation constants, an equilibrium between micropores and macropores, and the pH of the external solution (e.g. in macropore). To validate our model, we perform well controlled titration experiments for porous carbons. The model assumes that dry electrodes are initially electroneutral, and then upon submersion into an aqueous solution develop a net surface charge due to dissociation or adsorption of protons according the micropore-to-macropore equilibrium. We describe the model and present experimental data demonstrating very good agreement between predictions of initial and final pH of a solution after adding the activated carbon sample, and for final background concentrations of individual ionic species.

2. Theory

2.1. Multi-equilibria surface charge model

In recent work, Biesheuvel (2015) developed a model they termed amphoteric Donnan (amph-D) model which assumes carbon surfaces with a fixed (constant) value for positive and negative surface charges. Their model is based on the assumptions that (1) the concentrations of positive and negative surface charges are each fixed and independent of pH, and (2) each group has its own (independent) Donnan potential and micropore-to-macropore Boltzmann distribution. The result of this formulation is that surfaces are assumed to always adsorb both positive and negative ions from solutions at equal rates independent of solution pH.

In general, we recommend that models with constant surface charge (e.g. those that neglect the effects of pH on the degree of dissociation of surface charges) are not physical and have limited use in predicting adsorption capabilities across variations in pH and ionic strength. In the current work, we propose a model of surface groups based on first principles from weak electrolyte theory. We assume that the surfaces of micropores contain acid and base groups which can protonate or deprotonate according to their pK

values and in equilibrium with the solution within micropores. We then assume a standard Boltzmann type equilibrium between the solution in the micropores and the local solution outside of micropores. In this way, the charge density of positive surface groups and negative surface groups is a function of solution pH and ionic strength. Our formulation is general and can be used to study the adsorption properties of activated carbon with arbitrary number of immobile (acidic or basic) surface functional groups.

A schematic of our model is shown in Fig. 1. We assume n_X acidic surface groups and n_Y basic surface groups. Throughout this work, subscripts X and Y respectively correspond to acidic and basic surface functional groups. The degree of dissociation of functional groups (hence net chemical surface charge) is determined by the micropore pH environment and can be modeled with acid-base dissociation reactions for the form

$$X_iH \overset{K_{X_i}}{\rightleftharpoons} X_i^- + H_m^+ \quad (i = 1, \ldots, n_X) \tag{1}$$

$$Y_jH^+ \overset{K_{Y_j}}{\rightleftharpoons} Y_j + H_m^+ \quad (j = 1, \ldots, n_Y) \tag{2}$$

where X_iH is the i-th acidic functional group and Y_j is the j-th basic group. X_i^- and Y_jH^+ are the associated conjugate base and conjugate acid, respectively. H_m^+ represents hydronium ion in the micropores. K_{X_i} and K_{Y_j} are acid dissociation constants for the weak electrolytes and are defined as

$$K_{X_i} = c_{X_i^-}\, c_{m,H}/c_{X_iH}, \tag{3}$$

$$K_{Y_j} = c_{Y_j}\, c_{m,H}/c_{Y_jH^+}, \tag{4}$$

where $c_{X_i^-}$, c_{X_iH}, c_{Y_j}, and $c_{Y_jH^+}$ are volume-average concentration of functional groups (moles per micropore volume), and $c_{m,H}$ is hydronium micropore concentration. We follow Persat et al. (2009a) and use only the acid dissociation constants K_a (for both weak acid and weak base) and avoid using a base dissociation constant K_b (the subscript "a" is then dropped for this reason). For reference, K_a and K_b are related through $K_aK_b = K_w$, where K_w is the water autoprotolysis constant (10^{-14} M^2 at 25 °C).

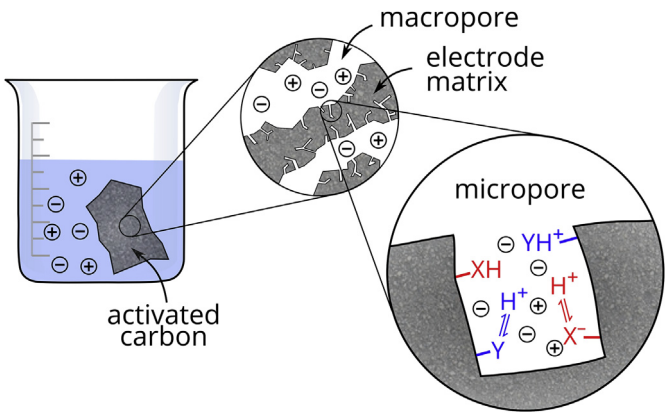

Fig. 1. Schematic of our acid-base equilibria model for activated carbon with bimodal (micropore and macropore) pores. Here, the carbon is electrically "floating" (not connected to an electrical source) and in equilibrium with the solution in a beaker. Electrolyte (outside carbon) and macropores (pathways for ion transport) are electroneutral. Micropores, however, are ion adsorbing regions wherein electronic, ionic, and surface charges (due to acid-base equilibrium) are in balance with zero net charge. We here depict a special case of one acidic and one basic surface functional group in the micropores. Note the global net neutrality of surface charges, charge in solution, and net surface electrons within the micropore.

The micropore volume is $v_m = p_m v_e$, where p_m is micropore porosity and v_e is (macroscopic) electrode volume. For amount (moles) of each site (X_i^-, Y_j, etc), one should multiply the concentrations shown here by the pore volume v_m. We further follow the convention of Persat et al. (2009a, 2009b) in which one only keeps track of hydronium (not hydroxide) ions in the formulations. Hydroxide concentration can, of course, be determined from the relation for water autoprotolysis in the bulk liquid, $c_{OH} = K_w/c_H$, and in the micropores, $c_{m,OH} = K_w/c_{m,H}$. The analytical concentration of each acidic or basic group ($c_{X_i,0}$ and $c_{Y_j,0}$) is a fixed value for the sample and is equal to sum of the concentrations of each ionization state of the functional group (see Persat et al. (2009a)). Hence, we write

$$c_{X_i,0} = N_{X_i,0}/v_m = c_{X_iH} + c_{X_i^-}, \tag{5}$$

$$c_{Y_j,0} = N_{Y_j,0}/v_m = c_{Y_jH^+} + c_{Y_j} \tag{6}$$

Note, the concentrations here are per micropore volume. $N_{X_i,0}$ and $N_{Y_j,0}$ are amount (moles) of acidic and basic groups of the sample, respectively. Chemical charge density of carbon (in units of Coulombs per micropore volume) is then

$$\begin{aligned}\sigma_{chem} &= \sum_i \sigma_{X_i^-} + \sum_j \sigma_{Y_jH^+} \\ &= -F\sum_i c_{X_i,0}\left(1 + \frac{c_{m,H}}{K_{X_i}}\right)^{-1} + F\sum_j c_{Y_j,0}\left(1 + \frac{K_{Y_j}}{c_{m,H}}\right)^{-1},\end{aligned} \tag{7}$$

where $\sigma_{X_i^-} = -Fc_{X_i^-}$ and $\sigma_{Y_jH^+} = Fc_{Y_jH^+}$ are surface charges associated with i-th acidic and j-th basic functional group, respectively, and F is Faraday's constant.

2.2. Electric double-layer model

We use an mD model in which the electric double layers (EDLs) in micropore volume are treated as strongly overlapping (Biesheuvel et al., 2011; Hemmatifar et al., 2015). This model thus assumes uniform ion concentration within the micropores. Concentration of protons in micropores can then be related to that of macropores assuming a micropore-to-macropore equilibrium following a Boltzmann distribution of the form

$$c_{m,H} = c_H \exp(-\Delta\phi_D/V_T), \tag{8}$$

where $\Delta\phi_D$ is Donnan potential drop between the micropores and the adjacent (local) electrolyte solution, and V_T is thermal voltage. By taking logarithm of both sides and multiplying by negative one, Eq. (8) can be transformed to

$$pH_m = pH + \frac{\Delta\phi_D}{\ln(10)V_T}, \tag{9}$$

where pH_m and pH are respectively the pH value at micropores and the (local) net neutral electrolyte within macropores. Eq. (9) shows that micropore pH value is linked with electrolyte pH through Donnan potential. Note that we explicitly assume the micropore pH (and not the electrolyte pH) directly determines the degree of dissociation of functional groups, although all quantities are coupled according to Eq. (9). Also, note the Donnan potential is only negligible in the high ionic strength limit. So, for a finite ionic strength electrolyte, the measurable pH (electrolyte pH) does not

by itself determine the degree of dissociation of functional groups. We discuss this in more detail in Section 4.1.

Throughout this paper, we assume a binary and fully dissociated salt such that

$$c_{m,\pm} = c_{\pm} \exp(-z_{\pm}\Delta\phi_D/V_T), \tag{10}$$

where subscripts + and − correspond to cationic and anionic species, respectively. So, $c_{m,+}$, for example, is the micropore concentration of the salt cation, and c_+ is electrolyte concentration of salt cation (outside the micropores) with valence z_+. The formulation here can easily be extended to arbitrary (non-binary) weak electrolytes in solution by taking into account the dissociation constant of dissolved species (similar to Eqs. (3) and (4)). Ionic charge density in the micropores (in units of Coulombs per micropore volume) can then be written as

$$\sigma_{ionic} = F\sum_k z_k\, c_{m,k}, \tag{11}$$

where the summation is over all ionic species ($k = H^+, OH^-, +, -$). The third form of charge (besides the chemical σ_{chem} and ionic σ_{ionic}) is the electronic charge. In the simplest form, electronic charge in carbon matrix adjacent to acidic or basic sites is a linear function of micropore potential drop $\Delta\phi_m$ (potential difference between electrode surface and center of micropore) as

$$\sigma_{elec} = C_m\ \Delta\phi_m, \tag{12}$$

where C_m is volumetric capacitance of micropores. Multiplying C_m by ν_m, we arrive at total capacitance of the carbon electrode. The chemical, ionic, and electronic charges add up to zero (charge compensation) as in

$$\sigma_{elec} + \sigma_{chem} + \sigma_{ionic} = 0. \tag{13}$$

The potential difference between carbon matrix and electrolyte solution (external voltage V_{ext}) is related to micropore potential and Donnan potential as

$$V_{ext} = \Delta\phi_m + \Delta\phi_D. \tag{14}$$

In the case of a single floating electrode (one electrode with no external voltage applied), electronic charge vanishes and we have $\sigma_{elec} = \Delta\phi_m = 0$. The voltage drop across electrode and electrolyte solution is then simply Donnan potential $\Delta\phi_D$.

2.3. Mass conservation

The model developed above is applicable in the case of negligible Faradaic reactions, i.e. carbon at zero or sufficiently low applied voltage. In this initial paper on our pH and surface charge model, we consider ion adsorption behavior of activated carbon electrodes disconnected from any power source and in equilibrium with a local solution as shown in Fig. 1. The sample is in contact with a (binary) electrolyte solution with initial cation concentration of $c_{+,0}$ and anion concentration of $c_{-,0}$ (see Fig. 1). We then seek a prediction of the finial concentration of species (c_+ and c_-), salt adsorption, micropore and electrolyte pH, and degree of dissociation of functional groups.

To begin, electroneutrality holds in the electrolyte in contact with the porous material such that

$$z_+c_+ + z_-c_- + c_H - K_w/c_H = 0. \tag{15}$$

Next is the mass conservation for individual ionic species (c_+ and c_- here). Upon the contact between carbon and electrolyte, the ions redistribute between the electrolyte and micropore volumes such that

$$\nu_{sol}\ c_{\pm,0} = (\nu_{sol} - \nu_m)\ c_{\pm} + \nu_m\ c_{m,\pm}, \tag{16}$$

where ν_{sol} is *total* volume of the electrolyte. For example, in a titration experiment, $\nu_{sol} = \nu^0_{sol} + \nu_{titrant}$, where ν^0_{sol} is *initial* volume of electrolyte and $\nu_{titrant}$ is volume of added titrant. The left-hand side of Eq. (16) is total amount (moles) of each ion. The first and second term in the right-hand side are moles of each ion present respectively in the electrolyte and in the acidic/basic micropores. Note that for binary salt, we can define micropore cationic and anionic salt adsorption as $\Gamma_{\pm} = \nu_m(c_{m,\pm} - c_{\pm,0})$. So, Γ_+ and Γ_- are respectively amount (in moles) of adsorbed cations and anions.

The set of equations in Sections 2.1–2.3 fully describe the steady state solution of the problem with c_H, c_+, c_-, $\Delta\phi_D$, and $\Delta\phi_m$ as unknowns. For our case of floating electrode, we drop Eq. (14) and set $\sigma_{elec} = 0$ and $\Delta\phi_m = 0$. Also, note that for the special case of ideal solution (infinite dilution) limit, c_+, $c_- \to 0$, and so $c_H = \sqrt{K_w}$ (pH = 7) in the electrolyte according to electroneutrality condition. The set of Eqs. (13) and (14) in ideal solution limit then result in non-trivial (non-zero) solutions for $\Delta\phi_D$, and $\Delta\phi_m$. We refer the reader to Section S-1 of the Supplementary Information (SI) for further discussion.

3. Materials and methods

3.1. Materials

We used a commercially available activated carbon cloth (ACC) (Zorflex FM50K, Calgon Carbon Corp., PA, USA) with 0.26 g cm^{-3} volumetric density. We modified pristine ACC with nitric acid (70% w/w, Sigma-Aldrich) solution to increase the surface acidity and to remove residual surface impurities as much as possible. To this end, we immersed ACC into nitric acid at room temperature for 2 h. We then rinsed ACC thoroughly with deionized water (DI) multiple times. The electrodes were soaked in DI overnight and dried at 150 °C in a convection oven. We used this nitric acid treated activated carbon cloth (N-ACC) in all experiments in this work.

3.2. Experimental setup

We prepared several solutions of NaCl with a wide pH range using 1 M HCl and NaOH stock solutions. To this end, we filled two sets of 14 containers (28 in total) with 20 mM NaCl solution (pH ~ 7, purged with nitrogen gas for 1 h) and added volumes of HCl or NaOH ranging from ~ 3 μL to ~ 1 mL to each container. The final volume of solution in each container was 25 mL. Our pH meter was an Omega PHE-3700 probe connected to a PHH-37 pH meter (Omega Engineering, CT, USA). The measured pH values of solutions were 1.76, 2.01, 2.25, 2.69, 3.01, 3.87, 5.62, 9.33, 10.83, 11.36, 11.61, 11.92, 12.16, and 12.41. We added 0.75 g of N-ACC to each container of the first set (sample solutions). No N-ACC was added to the second set (control solutions). Control and sample solutions were sealed and gently agitated for 14 h. We measured pH value and individual ion content of the solutions after this equilibration. Sodium and chloride ion contents were measured respectively by inductively coupled plasma mass spectrometry (ICP-MS X Series II, Thermo Scientific, MA, USA) and ion chromatography (DIONEX DX 500, DIONEX, CA, USA) at Stanford ICP-MS/TIMS Facility.

4. Results and discussion

4.1. Model results and physical insights

In this section, we focus on model predictions in an attempt to gain insight into salt adsorption and surface charge trends for carbon under various pH environments.

4.1.1. Effect of analytical concentration and pK's of surface groups on titration curves

First, we note that our model has $2(n_X + n_Y)$ free parameters ($c_{X_i,0}$, $c_{Y_j,0}$, K_{X_i}, and K_{Y_j} for $i = 1, \ldots, n_X$ and $j = 1, \ldots, n_Y$). To study the effect of each individual parameter, we model titration of carbon with a strong acid and base (i.e. HCl and NaOH) and compare it to blank titration (in absence of carbon). Although our model allows for arbitrary number of weak electrolyte groups, for simplicity, we use $n_X = 1$ and $n_Y = 1$, and consider dissociation reactions below

$$XH \overset{K_X}{\rightleftharpoons} X^- + H_m^+ \tag{17}$$

$$YH^+ \overset{K_Y}{\rightleftharpoons} Y + H_m^+ \tag{18}$$

Fig. 2 shows titration curves for four types of carbon, each with a single surface functional group with a fixed pK_X or pK_Y. Two carbon samples have each a single acidic surface group with $pK_X = 4$ or 10 (Fig. 2a and b). The two others have each a basic surface group with $pK_Y = 4$ or 10 (Fig. 2c and d). For each case, we show the results for three values of $c_{X,0}$ or $c_{Y,0}$, namely, 0.1, 0.5, and 1 M (solid lines). Dashed lines show blank titration curves. We here used an initial salt concentration $c_0 = 20$ mM, final solution volume $v_{sol} = 25$ mL, and titrant concentration of $c_{stock} = 1$ M (same for acid and base titrants). Other parameters used to generate these plots are listed in Table 1. Refer to Section S-2 of the SI for details of this titration model. Fig. 2 summarizes basic features of model predictions which are very useful in interpreting titration experiments. In particular, the qualitative shape of titration curves help us individually identify if a sample has primarily weak acid groups, primarily weak basic groups, multiple weak acid, multiple weak bases, or combination of weak acids or weak bases. For example, when titrated with base, the acidic carbon (Fig. 2a and b) result in a negative surface charge. The deprotonation of the surface charge, through

Table 1
Model parameters used in titration model and Fig. 2.

Parameter	Description	Value	Unit
v_m	Micropore volume	0.5	mL
m_e	Electrode mass	0.75	g
v_{sol}^0	Initial volume of solution	25	mL
c_{stock}	Titrant (HCl, NaOH) stock concentration	1000	mM
z_+, z_-	Cation and anion valence	1	–

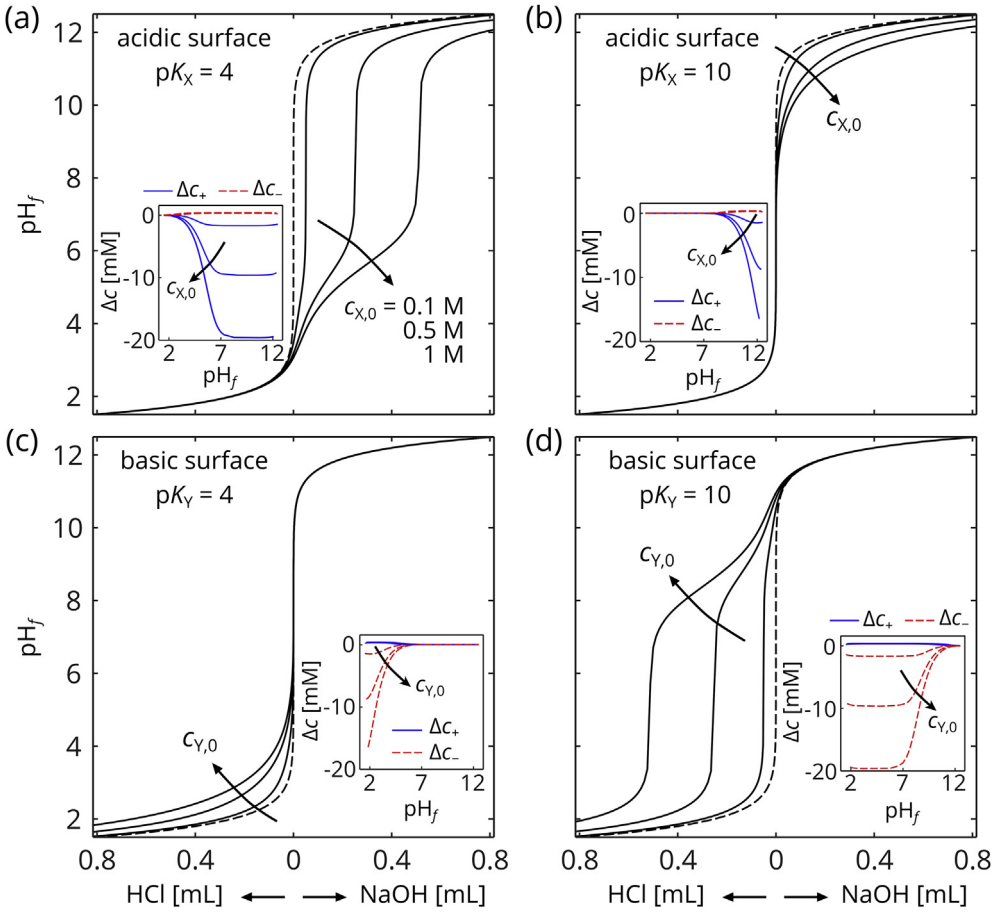

Fig. 2. Summary of characteristic shapes of predicted titration curves for samples with weak acids and weak bases for porous carbon samples. (a) and (b) each consider a single acidic functional group, and respective pK_X are 4 and 10, while (c) and (d) each consider a single basic functional group with respective pK_Y of 4 and 10. Titrants are 1 M HCl and 1 M NaOH. We show results for $c_{X,0}$, $c_{Y,0} = 0.1$, 0.5, and 1 M (solid lines). Dashed lines indicate blank titrations ($c_{X,0} = c_{Y,0} = 0$). Insets show change in concentration of anion/cation ($\Delta c_\pm = c_\pm - c_{\pm,0}$) as a function of pH_f. Initial salt concentration and solution volume are $c_0 = 20$ mM and $v_{sol} = 25$ mL. Other parameters are listed in Table 1.

macropore-to-micropore equilibrium, drives a net recruitment of cations from solution and tend to lower the final pH of the solution (pH_f). Titrating an acidic surface sample with strong acid, results in negligible effect on pH curve of the titration as expected. We also note that higher values of the analytical concentration of the weak acid $c_{X,0}$ result in a stronger decrease in pH compared to blank titration. Comparison of Fig. 2a and b, highlights the effect of the absolute value of pK of the acidic group. Note how a more acidic (lower pK) surface group results in a more profound departure of the titration curve from the blank at mid-range pH values.

The insets of Fig. 2a and b show change in concentration of univalent anions and cations in the solution outside of the micropores ($\Delta c_{\pm} = c_{\pm} - c_{\pm,0}$) versus pH_f. Here, $c_{\pm,0}$ is initial concentration of species (right after addition of titrant), and $c_{\pm}$ is their concentration after carbon and electrolyte are equilibrated. As expected, we observe preferential adsorption of cations at $pH_f > pK_X$ and negligible expulsion of anions throughout the titration. Moreover, the cation adsorption increases with analytical concentration of acidic groups $c_{X,0}$ (see arrows). Titration of basic carbon (Fig. 2c and d) with strong acid, on the other hand, results in pH_f values higher than blank curve and a net positive surface charge. This departure from blank is pronounced for $pH_f < pK_Y$.

We again stress that K_Y and pK_Y are the *acidic K* and pK of weak base Y (see Eq. (4) for definition). For example, a stronger weak base Y corresponds to lower K_Y and higher pK_Y value. The insets of Fig. 2c and d show adsorption of anions at $pH_f < pK_Y$ and negligible expulsion of cations throughout the titration. The anion adsorption here is primarily due to net positive surface charge of basic carbon.

The preferential adsorption of cations and anions is directly due to the ability of acidic and basic functional groups to protonate or deprotonate according to their pK value. As an example, the model developed by Biesheuvel et al. (2015), would predict constant and equal values of anion versus cation adsorption (and thus constant net salt adsorption) independent of pH. We discuss the ion adsorption in more detail in the next section.

4.1.2. *Effect of ionic strength on macropore-to-micropore equilibrium*

We here explore the effect of ionic strength on pH variations and surface chemical charge in the current model. Fig. 3a shows final pH of micropore ($pH_{m,f}$) versus final pH of solution (pH_f) for initial salt concentrations in the range of 0–500 mM (solid lines). We assume titration of a carbon with one acidic ($c_{X,0} = 1$ M, $pK_X = 4$) and one basic ($c_{Y,0} = 1$ M, $pK_Y = 10$) surface group. Other parameters used are identical to those of Fig. 2. Dashed line shows where $pH_{m,f} = pH_f$. Note that intersection of solid and dashed lines is actually the pH of the PZC (pH_{PZC}), which also corresponds to a pH where $\Delta\phi_D = 0$ and $\sigma_{chem} = 0$. Results show that $pH_{m,f}$ is lower (higher) than pH_f above (below) pH_{PZC}. The surface functional groups of micropore (which act as weak electrolyte) oppose variations in $pH_{m,f}$ compared to pH_f. Further, we note that $pH_{m,f}$ approaches pH_f only at high ionic strengths. This is a feature not observed in simple buffers and is strictly resulting from the macropore-to-micropore equilibrium. As we will discuss later in this section, this dependence on ionic strength is indicative of a shift in the adsorption dynamics from net salt adsorption to ion swapping. Also, note that as per Eq. (8), the Donnan potential $\Delta\phi_D$ approaches zero in the limit of high ionic strength.

The difference between $pH_{m,f}$ and pH_f implies that the measured pH of electrolyte (pH_f) may not accurately represent micropore environment, and consequently, surface pK and surface charge. We illustrate this in Fig. 3b and c, where we plot concentration of charged acidic and basic groups (c_{X^-} and c_{YH^+}) as a function of pH_f and $pH_{m,f}$. When plotted against $pH_{m,f}$, c_{X^-} and c_{YH^+} artificially appear to be strong functions of initial salt concentration c_0 (see Fig. 3b). Note that the *observed* pK's (half-dissociation points) in this case approach the actual values ($pK_X = 4$ and $pK_Y = 10$) only in the limit of $c_0 \to \infty$. On the other hand, Fig. 3c shows that all c_{X^-} and c_{YH^+} curves collapse when plotted against $pH_{m,f}$ on which they depend strongly.

We note that dissociation constants are here assumed to be constant. Ideally, dissociation constants are corrected for ionic strength, for example using a Davies-type equation (Persat et al., 2009a). Further, dissociation constants might be functions of carbon electric potential as well. We chose to not to adopt such corrections in this work in order to simplify the presentation and because (1) our current focus is the effect of ionic strength on differences in electrolyte and micropore environments through

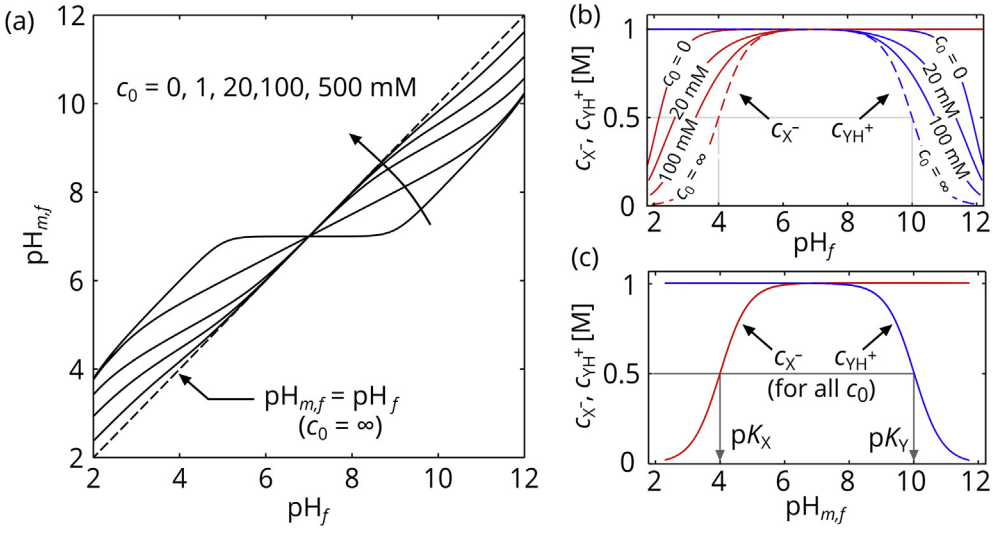

Fig. 3. Ionic strength affects the equilibrium between carbon micropores and the electrolyte (outside the micropore). (a) Final micropore pH ($pH_{m,f}$) versus final electrolyte pH (pH_f) for titration model with c_0 = 0, 1, 20, 100, and 500 mM. Surface parameters are $c_{X,0} = 1$ M, $pK_X = 4$, $c_{Y,0} = 1$ M, and $pK_Y = 10$, and other parameters are similar to those of Fig. 2. $pH_{m,f}$ is lower (higher) than pH_f above (below) PZC ($pH_{PZC} = 7$ here), and $pH_{m,f}$ approaches pH_f only at high ionic strengths. (b) Concentration of charged acidic and basic groups (c_{X^-} and c_{YH^+}) versus pH_f and (c) versus $pH_{m,f}$. Curves for c_{X^-} and c_{YH^+} collapse onto a single curve when plotted against $pH_{m,f}$, as per our formulation.

adsorption process, and (2) the applicability of the Davies equation for correction of pK values within a micropore (and overlapped double layers) is an open question. We hope to study this further in future work.

Throughout this section (Section 4.1), for simplicity of presentation, we considered a *symmetric* case for carbon with $c_{X,0} = c_{Y,0}$, $pK_X = 4$, and $pK_Y = 10$. Hence, the results are symmetric around $pH_{PZC} = 7$. In Section S-3 of the SI, we present the results for an *asymmetric* carbon with $c_{X,0} = c_{Y,0}$ and $pK_X = 4$ (as before), but with $pK_Y = 8$.

4.1.3. Determination of point of zero charge

As mentioned earlier, PZC corresponds to $\sigma_{chem} = 0$ and $\Delta\phi_D = 0$. We here discuss the effect of dissociation constant of surface groups and their concentrations as well as ionic strength on pH_{PZC} for a simple case of one acidic and one basic surface functional group. We also provide insights for the general case. PZC in our simple case requires

$$-\frac{c_{X,0}}{1+c_H/K_X}+\frac{c_{Y,0}}{1+K_Y/c_H}=0, \tag{19}$$

which can be recast as a quadratic equation in c_H with a unique real positive root (from Descartes' rule of signs). The first term in Eq. (19) is the (negative) surface charge associated with acidic group (σ_{X^-}), and the second term is (positive) charge due to basic group (σ_{YH^+}). By assuming fixed dissociation constants, Eq. (19) and hence pH_{PZC} are independent of ionic strength (see Fig. 3a). For a general case of n_X acidic and n_Y basic groups, the resulting equation is a polynomial of degree $n_X + n_Y$. We solve Eq. (19) for $c_{X,0} > c_{Y,0}$ and $c_{X,0} < c_{Y,0}$, take the logarithm of the solution, and arrive at

$$pH_{PZC} = \begin{cases} pK_X - \log\alpha_1 - \log\varepsilon & c_{X,0} > c_{Y,0} \\ pK_Y + \log\alpha_2 + \log\varepsilon & c_{X,0} < c_{Y,0} \end{cases}, \tag{20}$$

where $0 < \alpha_1 = c_{X,0}/c_{Y,0} - 1$ and $0 < \alpha_2 = c_{Y,0}/c_{X,0} - 1$, and ε can be written as

$$\varepsilon = \frac{1}{2}\left(1+\sqrt{1+4(\alpha+1)/\alpha^2\cdot K_Y/K_X}\right), \tag{21}$$

where α is either α_1 or α_2 (both result in the same value of ε). Eq. (20) generalizes the effect of individual pK's and analytical concentrations ($c_{X,0}$ and $c_{Y,0}$) on PZC. In special case of $c_{X,0} = c_{Y,0}$ (i.e. in the limit of $\alpha_1, \alpha_2 \to 0$), we arrive at the simple result that $pH_{PZC} = (pK_X + pK_Y)/2$ (which may be familiar to readers experienced in buffer calculations). In Fig. S.3 of the SI, we show pH_{PZC} as a function of α_1 and α_2 for $pK_X = 4$ and $pK_Y = 10$. We show that pH_{PZC} decreases with α_1 (where $c_{X,0} > c_{Y,0}$) and increases with α_2 (where $c_{X,0} < c_{Y,0}$), and further demonstrate that, for $\alpha_1 \gg \alpha_0$ (where α_0 is some threshold that depends solely on pK_X and pK_Y), ε approaches unity and according to Eq. (20), pH_{PZC} is independent of pK_Y. In the case where $\alpha_2 \gg \alpha_0$, ε approaches unity but then pH_{PZC} is independent of pK_X. Refer to Section S-4 of the SI for more information. These observations help in quick estimates of pH_{PZC} given some knowledge of surface pK values.

4.1.4. Chemical charge efficiency: a new parameter for salt removal efficiency due to surface charge

Lastly, we discuss the effect of pH and ionic strength on adsorption mechanisms and define parameters to identify them. Fig. 4a shows net salt adsorbed Γ as a function of $pH_{m,f}$ for a carbon with one acidic ($c_{X,0} = 1$ M, $pK_X = 4$) and one basic ($c_{Y,0} = 1$ M, $pK_Y = 10$) surface groups at various initial salt concentration c_0 in the range of 0–500 mM. Other parameters used are identical to those of Fig. 2. Salt removal Γ (in units of moles) for a univalent electrolyte is calculated as

$$\Gamma = \Gamma_+ + \Gamma_- = \nu_m\left((c_{m,+} - c_{+,0}) + (c_{m,-} - c_{-,0})\right), \tag{22}$$

where Γ_+ and Γ_- are cationic and anionic salt adsorption (sodium and chloride ions, for instance). We stress that $c_{+,0}$ and $c_{-,0}$ differ from initial salt concentration c_0. These are theoretical cation and anion concentrations the solution would obtain without carbon-electrolyte equilibration, while c_0 is an initial salt concentration in the absence of added titrant. Results show considerable salt adsorption at $pH_{m,f} < pK_X$ and $pH_{m,f} > pK_Y$ and much lower adsorption otherwise. This expected trend is in accordance with higher net negative (positive) micropore surface charge at pH values lower (higher) than pK_X (pK_Y). In Section 4.1.1, we show experimental results which support this observation. Fig. 4a also shows that at a fixed pH environment (fixed $pH_{m,f}$), salt adsorption Γ decreases with increase in c_0 (or equivalently, initial ionic strength). For example, at $pH_{m,f} = 3$, salt adsorption is almost halved when initial salt concentration increases from 20 to 500 mM. This result can be attributed to a higher degree of expulsion of co-ions (ions with like charge relative to that of surface groups) at higher initial concentrations. At lower salt concentrations, co-ion expulsion is less important than counter-ion recruitment into the micropore. The two insets of Fig. 4a illustrate this point. The insets show individual cationic and anionic salt adsorption Γ_+ and Γ_- for $c_0 = 20$ and 500 mM cases. At low ionic strengths, counter-ion adsorption (i.e. adsorption of cations at high $pH_{m,f}$ and anions at low $pH_{m,f}$) dominates relative to co-ion expulsion. For example, $\Gamma_+ \gg |\Gamma_-|$ at $pH_{m,f} = 11$ and $|\Gamma_+| \ll \Gamma_-$ at $pH_{m,f} = 3$. Conversely, at high ionic strengths corresponding to small Donnan potentials, counter-ion adsorption and co-ion expulsion are of the same order ($|\Gamma_+| \approx |\Gamma_-|$). In other words, low ionic strength can be associated with counter-ion recruitment and salt adsorption, while high ionic strength leads to increased ion swapping. We here propose a characterization of this effect by defining a signed "chemical charge efficiency" parameter as

$$\Lambda_{chem} = \frac{F\Gamma}{\Sigma_{chem}} = \frac{F(\Gamma_+ + \Gamma_-)}{\nu_m\sigma_{chem}}, \tag{23}$$

where $\Sigma_{chem} = \nu_m\sigma_{chem}$ is net micropore surface charge in units of Coulombs. Fig. 4b shows chemical charge efficiency as a function of $pH_{m,f}$ for parameters identical to those of Fig. 4a. Results show that at $pH_{m,f} = pH_{PZC}$, $\Lambda_{chem} = 0$, and associated zero anion or cation adsorption. At $pH_{m,f} > pH_{PZC}$, cation adsorption is greater than anion expulsion ($\Gamma_+ > |\Gamma_-|$), and the surface charge is positive ($\Sigma_{chem} > 0$), and hence $\Lambda_{chem} > 0$. At $pH_{m,f} < pH_{PZC}$, however, cation adsorption is lower than anion expulsion ($|\Gamma_+| < \Gamma_-$), surface charge is negative ($\Sigma_{chem} < 0$), and so $\Lambda_{chem} < 0$. Further, chemical charge efficiency approaches unity (in magnitude) at low ionic strengths, since counter-ion adsorption is much greater than co-ion expulsion. For $pH_{m,f}$ values very close to pH_{PZC}, however, chemical charge density and adsorbed salt both vanish. At this limit, adsorbed salt Γ approaches zero faster than surface charge Σ_{chem} (in magnitude) such that chemical charge efficiency ($F\Gamma/\Sigma_{chem}$ ratio) approaches zero (see Fig. 4.). We note that negative chemical charge efficiency here does not mean ion expulsion dominates ion adsorption (note, $\Gamma > 0$ for all ionic strengths after all), nor does it imply that electrolyte ionic strength (outside carbon micropores) increases to a higher value. A negative chemical charge efficiency simply indicates that net micropore surface charge Σ_{chem} (or equivalently, surface chemical charge density σ_{chem}) is negative.

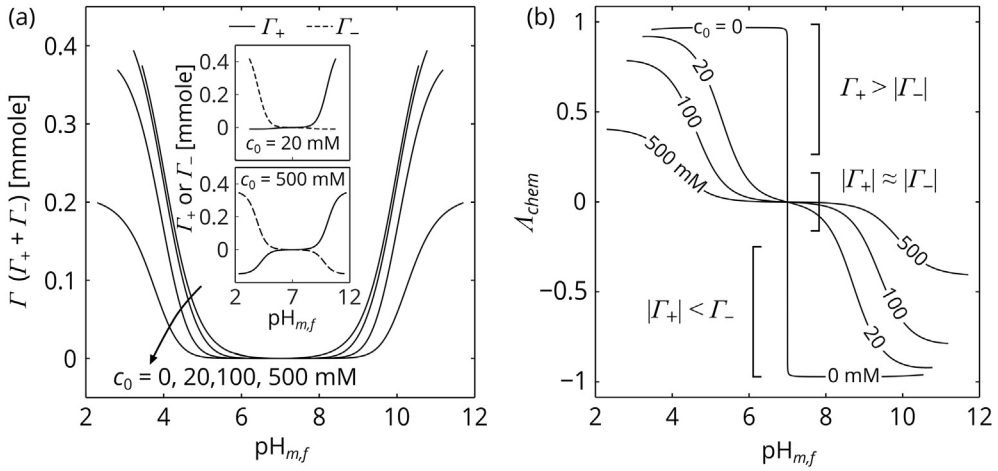

Fig. 4. Effect of ionic strength and micropore pH environment on salt adsorption dynamics. (a) Net adsorbed salt $\Gamma = \Gamma_+ + \Gamma_-$ as a function of $pH_{m,f}$ for a carbon with one acidic ($c_{X,0} = 1$ M, $pK_X = 4$) and one basic ($c_{Y,0} = 1$ M, $pK_Y = 10$) surface groups for $c_0 = 0$, 20, 100, and 500 mM. Other parameters are identical to those of Fig. 2. Salt adsorption is considerable at $pH_{m,f} < pH_X$ and $pH_{m,f} > pH_Y$. Further, the magnitude of salt adsorption decreases with increasing ionic strength (or equivalently with increasing c_0). The insets show individual cationic and anionic salt adsorption (Γ_+ and Γ_-) for $c_0 = 20$ and 500 mM. (b) Chemical charge efficiency versus $pH_{m,f}$ for the same c_0 values as in (a). At low ionic strengths, counter-ion adsorption (cations at high $pH_{m,f}$ and anions at low $pH_{m,f}$) dominates co-ion expulsion and so $|\Lambda_{chem}| \to 1$. At high ionic strengths, however, counter-ion adsorption and co-ion expulsion are of the same order (ion swapping) and hence $\Lambda_{chem} \to 0$.

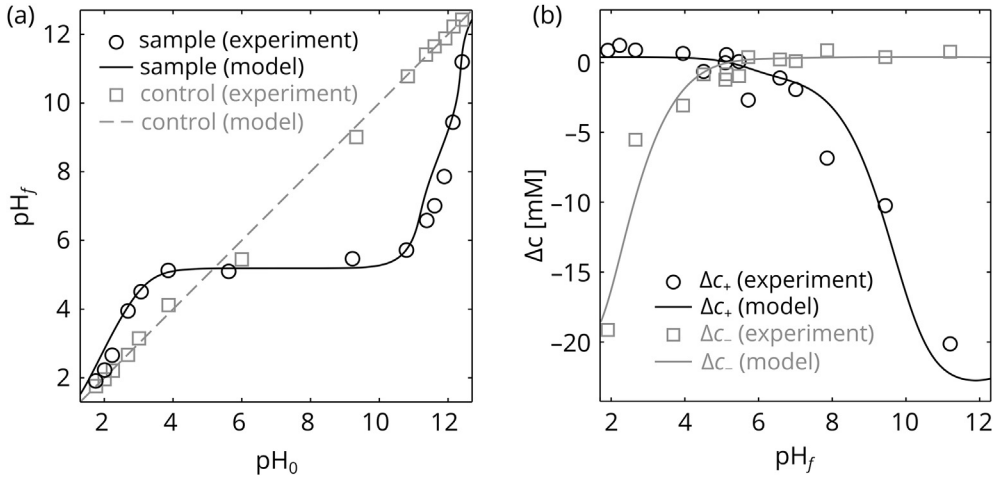

Fig. 5. Model and experimental results of pH shift and ion adsorption. (a) Final electrolyte pH (pH_f) versus initial pH (pH_0) for N-ACC samples (circles), control samples (squares), and fitted model (solid line). Dashed line shows $pH_f = pH_0$. pH_f for N-ACC samples is higher than pH_0 for $pH_0 < 5$, and is lower than pH_0 for $pH_0 > 5$. N-ACC therefore is an ion adsorbent with $pH_{PZC} \sim 5$. (b) Change in concentration of sodium and chloride ions versus pH_f for experiments and fitted model. Results show specific adsorption of chloride ions at $pH_f < pH_{PZC}$ and strong adsorption of sodium ions otherwise. We modeled N-ACC with $c_{X,0} = 1.17$ M, $c_{Y,0} = 1.1$ M, $pK_X = 4$, and $pK_Y = 8$. Other parameters used in the model are listed in Table 2.

4.2. Experimental results and model verification

As described in Section 3.2, we prepared 28 containers of NaCl solutions with a wide pH range by adding 1 M HCl or NaOH to 20 mM NaCl electrolyte. Measured pH values were in the range of 1.76–12.41 and final volume of each container was 25 mL. We added 0.75 g of N-ACC samples to half of the containers. The rest of containers were used as control (no N-ACC added). We measured final pH value and individual ion concentration of the solutions after 14 h agitation.

Fig. 5a shows final pH of electrolyte (pH_f) as a function of initial pH of solution (pH_0) for both experiments and model. Circle and square markers show the results for N-ACC samples and control experiments, respectively. Dashed line represents $pH_f = pH_0$. Control experiments (square markers) very closely follow the dashed line, indicating trace dissolved carbon dioxide results in a minimal drift in pH (all samples purged with nitrogen gas and carefully sealed). Solutions with N-ACC samples (circle markers), however, noticeably deviate from dashed line. pH_f is higher than pH_0 for pH values below ~ 5, and is lower than pH_0 for pH values above ~ 5. This suggests that N-ACC has $pH_{PZC} \sim 5$, as it behaves as a base at $pH_0 < 5$ and behaves as acid at $pH_0 > 5$. Fig. 5b shows change in concentration of sodium and chloride ions versus pH_f for the same experiments as in Fig. 5a. Results show strong adsorption of chloride ions at low pH ($pH_f < 5$) and strong adsorption of sodium ions otherwise.

Based the experimental measurements above, and for simplicity, we modeled N-ACC surface as an ion adsorbent with one acidic and one basic group. Solid lines in Fig. 5a and b show the model predictions using $c_{X,0} = 1.17$ M, $c_{Y,0} = 1.1$ M, $pK_X = 4$, and $pK_Y = 8$ as free parameters. We found values of free parameters by minimizing the absolute value of the error between experiments

Table 2
Parameters used in model for N-ACC samples.

Parameter	Description	Value	Unit
$c_{X,0}$	Analytical concentration of acidic group	1.17	M
$c_{Y,0}$	Analytical concentration of basic group	1.1	M
pK_X	pK value of acidic group	4	–
pK_Y	pK value of basic group	8	–
v_m	Micropore volume	0.5	mL
v_e	Electrode volume	2.9	mL
m_e	Electrode mass	0.75	g
v_{sol}	Final volume of solution	25	mL
c_{stock}	Titrant (HCl, NaOH) stock concentration	1000	mM
z_+, z_-	Cation and anion valence	1	–
c_0	Initial salt concentration	20	mM

and model. We list the parameters and other constants used in Table 2. Results show a good agreement between experiments and model and suggest that a simple two pK model can predict pH shifts and ion adsorption characteristics of N-ACC samples. Goodness of fit to the model is evaluated using coefficient of determination (R^2). R^2 is 0.95 and 0.998 for sample and control experiments (Fig. 5a) and is 0.94 and 0.93 for cation and anion concentration change (Fig. 5b).

4.3. Prediction of N-ACC surface charge

We used the fitted model above to estimate the surface charge of N-ACC samples. Fig. 6a shows surface charge density (σ_{chem}) as well as its associated acidic and basic surface charges (σ_{X^-} and σ_{YH^+}) as a function of micropore pH ($pH_{m,f}$). We here used $c_0 = 20$ mM (similar to experiments). Other c_0 values result in identical curves. We again stress that c_0 is initial dissolved salt concentration in the absence of added titrant. Fig. 6b shows σ_{X^-}, σ_{YH^+}, and σ_{chem} as a function of final electrolyte pH (pH_f) for c_0 values in the range of 0–500 mM. This figure shows that when plotted against pH_f, surface charges (σ_{X^-}, σ_{YH^+}, and σ_{chem}) artificially appear to be strong functions of initial salt concentration c_0. Left and right axes show surface charge densities in units of C cm^{-3} and M, respectively. Note that $\sigma_{chem} = \sigma_{X^-} + \sigma_{YH^+}$ according to Eq. (7). The magnitudes of σ_{X^-} and σ_{YH^+} each strictly decrease with pH_f and result in a net positive surface charge for $pH_f < 5$ and net negative charge for $pH_f > 5$. This is in accordance with specific adsorption of anions (cations) at pH_f values lower (higher) than ~ 5 observed in experiments. Other parameters used in calculation of charge densities are listed in Table 2.

We note that in CDI operation, the electrodes usually experience voltage windows of around −1.2 to 1.2 V. This applied voltage range has been shown (He et al., 2016; Lee et al., 2010) to profoundly change pH of effluent solution (up to 5 units). Therefore, since surface charge density σ_{chem} is pH dependent, it inevitably varies in a CDI cycle. This highlights the importance of CDI models where surface charge is allowed to vary based on surface dissociation constants.

4.4. Proposed generalization for charge efficiency of CDI systems

We here present a proposed generalization of the often cited and reported charge efficiency parameter for CDI systems. The charge efficiency is typically defined as ratio of adsorbed salt to electronic charge as in $F\Gamma/\Sigma_{elec}$ (Cohen et al., 2011; Gao et al., 2014; Hemmatifar et al., 2015; Zhao et al., 2010), where $\Sigma_{elec} = v_m\sigma_{elec}$ is electronic charge in units of Coulombs. However, the common expressions for charge efficiency are only function of external voltage, initial salt concentration, and electrode capacitance, and thus do not account for surface charge effects. Hence, we here propose the following generalization for charge efficiency including functional groups with surface dissociation constants (pK). For simplicity, we assume that the electrolyte volume is large enough such that (1) initial and final electrolyte salt concentrations are approximately equal to each other and constant ($c_+ = c_{+,0}$ and $c_- = c_{-,0}$), (2) initial and final pH of electrolyte are equal, and (3) pH is moderate (4–10) (Persat et al., 2009a) such that salt anion (cation) concentration is considerably larger than hydronium (hydroxide) concentrations (e.g., salt concentration in CDI is typically 10–100 mM whereas $c_H = 0.1$ mM at pH = 4). We then substitute Eqs. (7), (11), and (12) into Eq. (13) and solve for $\Delta\phi_D$. Salt concentration Γ can now be written as $2c_0v_m(\cosh(\Delta\phi_D/V_T) - 1)$ (see Eq. (22)). Refer to Section S-5 of the SI for more detailed derivations. We then define the generalized charge efficiency as

$$\Lambda = \frac{F(\Gamma - \Gamma_{PZC})}{\Sigma_{elec}} = \frac{2Fc_0v_m}{C_m}\cdot\frac{\cosh(\Delta\phi_D/V_T) - \cosh(V_{PZC}/V_T)}{V_{ext} - \Delta\phi_D}, \tag{24}$$

where Γ_{PZC} is salt adsorbed at potential of zero charge V_{PZC} (i.e. potential at which $\Sigma_{elec} = 0$) and can be written as $2c_0v_m(\cosh(V_{PZC}/V_T) - 1)$. Note that charge efficiency is now a function of external voltage, initial pH, ionic strength (or c_0), and surface properties (i.e. $c_{X,0}$, $c_{Y,0}$, pK_X, and pK_Y). We also note that

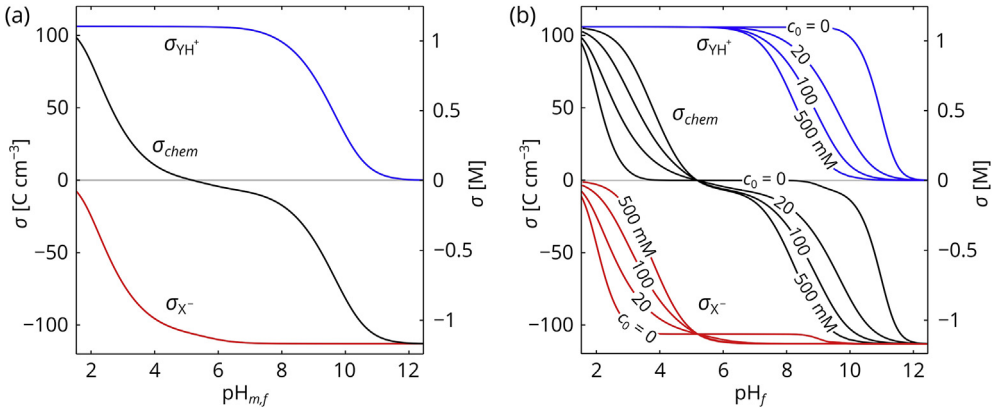

Fig. 6. Prediction of net, acidic, and basic surface charge densities (σ_{chem}, σ_{X^-}, and σ_{YH^+}) of N-ACC samples in units of C cm^{-3} (left axis) and M (right axis) versus (a) micropore pH ($pH_{m,f}$) and (b) final electrolyte pH (pH_f). Net surface charge density is sum of acidic and basic surface densities. pH_{PZC} (where $\sigma_{chem} = 0$) is ~ 5 for our N-ACC. Parameters used in calculation of charge densities are listed in Table 2.

due to presence of surface charge, it is possible for Γ to have a non-zero value when $\Sigma_{elec} = 0$ (i.e. at point of zero charge). Hence, Eq. (24) defines generalized charge efficiency in terms of the salt adsorbed relative to a base value of Γ_{PZC} . Hence, we formulate in terms of the difference $\Gamma - \Gamma_{PZC}$ in the numerator (this also ensures that the quantity Λ is bounded). In Section S-5 of the SI, we show plots of adsorbed salt and electronic charge as well as generalized charge efficiency vs V_{ext} in the range of −0.5 to 0.5 V. We present these results and formulation as a purely theoretical description of generalized charge efficiency which we hope to experimentally validate as part of future work, including experiments of full CDI cells with electrodes with significant surface charge.

5. Conclusions

We here expanded the current CDI-based surface charge models by coupling the mD model with weak electrolyte acid-base equilibria theory. Our model is based on a more physical treatment of the surface functional groups wherein the surface groups can protonate or deprotonate based on their individual pK values and micropore pH environment. Our formulation is applicable to arbitrary number of immobile (acidic or basic) surface functional groups. We applied our model to titration of activated carbon and showed (1) specific adsorption of cations and expulsion of anions at electrolyte pH values higher than pK of acidic groups, and (2) specific adsorption of anion and expulsion of cations at pH values lower than pK of basic groups. We studied equilibrium between micropores and macropores and proposed a model wherein micropore pH (and not directly the electrolyte pH) directly determines the degree of dissociation of functional groups. Hence, the electrolyte pH alone does not reflect ionization state of functional groups. This feature is strictly resulting from the macropore-to-micropore equilibrium and is not observed in simple buffers calculations. We further showed that this equilibrium is ionic strength dependent and is indicative of a shift in the adsorption dynamics from net salt adsorption to ion swapping. We introduced a new parameter we call *chemical charge efficiency* and showed that (1) it approaches unity (in magnitude) at low ionic strengths, where counter-ion adsorption dominates co-ion expulsion, and (2) it vanishes at high ionic strengths, where counter-ion adsorption and co-ion expulsion are of the same order (ion swapping). We validated our model by comparing predictions to experimental measurements from well controlled titration experiments of N-ACC samples. We measured initial and final pH of electrolyte after adding N-ACC samples as well as initial and final concentrations of individual ionic species (sodium and chloride) inductively coupled plasma mass spectrometry (ICP-MS) and ion chromatography (IC). Our fitted model with one acidic and one basic surface group showed a very good agreement with the experiments (with $c_{X,0} = 1.17$ M, $c_{Y,0} = 1.1$ M, p$K_X = 4$, and p$K_Y = 8$). Results showed strong adsorption of chloride ions at $pH_f < 5$ and strong adsorption of sodium ions otherwise. Finally, we used our model to estimate the surface charge of N-ACC samples and showed that net surface charge is negative (acidic) at $pH_f < 5$ and is positive (basic) otherwise.

Acknowledgements

This work was supported jointly by LLNL LDRD project 15-ERD-068 and TomKat Center for Sustainable Energy at Stanford University. Work at LLNL was performed under the auspices of the US DOE by LLNL under Contract DE-AC52-07NA27344. J.G.S., A.H., D.I.O., and J.W.P gratefully acknowledge support from TomKat Center for Sustainable Energy at Stanford University. A.H. also gratefully acknowledges the support from the Stanford Graduate Fellowship program of Stanford University.

Appendix A. Supplementary data

Supplementary data related to this article can be found at http://dx.doi.org/10.1016/j.watres.2017.05.036.

References

Andelman, M., 2014. Ionic group derivitized nano porous carbon electrodes for capacitive deionization. J. Mater. Sci. Chem. Eng. http://dx.doi.org/10.4236/msce.2014.23002.

Avraham, E., Noked, M., Cohen, I., Soffer, A., Aurbach, D., 2011. The dependence of the desalination performance in capacitive deionization processes on the electrodes PZC. J. Electrochem. Soc. 158, P168. http://dx.doi.org/10.1149/2.078112jes.

Babić, B.M., Milonjić, S.K., Polovina, M.J., Kaludierović, B.V., 1999. Point of zero charge and intrinsic equilibrium constants of activated carbon cloth. Carbon N. Y. 37, 477–481. http://dx.doi.org/10.1016/S0008-6223(98)00216-4.

Barkauskas, J., Dervinyte, M., 2004. An investigation of the functional groups on the surface of activated carbons. J. Serbian Chem. Soc. 69, 363–375. http://dx.doi.org/10.2298/JSC0405363B.

Bhatnagar, A., Hogland, W., Marques, M., Sillanpää, M., 2013. An overview of the modification methods of activated carbon for its water treatment applications. Chem. Eng. J. 219, 499–511. http://dx.doi.org/10.1016/j.cej.2012.12.038.

Biesheuvel, P.M., Bazant, M.Z., 2010. Nonlinear dynamics of capacitive charging and desalination by porous electrodes. Phys. Rev. E - Stat. Nonlinear, Soft Matter Phys. 81, 1–12. http://dx.doi.org/10.1103/PhysRevE.81.031502.

Biesheuvel, P.M., Fu, Y., Bazant, M.Z., 2011. Diffuse charge and Faradaic reactions in porous electrodes. Phys. Rev. E 83, 61507. http://dx.doi.org/10.1103/PhysRevE.83.061507.

Biesheuvel, P.M., Limpt, B. Van, Wal, A Van Der, van Limpt, B., van der Wal, A., 2009. Dynamic adsorption/desorption process model for capacitive deionization. J. Phys. Chem. C 113, 5636–5640. http://dx.doi.org/10.1021/jp809644s.

Biesheuvel, P.M., 2015. Activated carbon is an electron-conducting amphoteric ion adsorbent. arXiv preprint arXiv:1509.06354.

Biesheuvel, P.M., Suss, M.E., Hamelers, H.V.M., 2015. Theory of water desalination by porous electrodes with immobile chemical charge. Colloids Interface Sci. Commun. 9, 1–5. http://dx.doi.org/10.1016/j.colcom.2015.12.001.

Cohen, I., Avraham, E., Noked, M., Soffer, A., Aurbach, D., 2011. Enhanced charge efficiency in capacitive deionization achieved by surface-treated electrodes and by means of a third electrode. J. Phys. Chem. C 115, 19856–19863. http://dx.doi.org/10.1021/jp206956a.

Corapcioglu, M.O.O., Huang, C.P.P., 1987. The adsorption of heavy metals onto hydrous activated carbon. Water Res. 21, 1031–1044. http://dx.doi.org/10.1016/0043-1354(87)90024-8.

Gao, X., Omosebi, A., Holubowitch, N., Landon, J., Liu, K., 2017. Capacitive deionization using alternating polarization: effect of surface charge on salt removal. Electrochim. Acta 233, 249–255. http://dx.doi.org/10.1016/j.electacta.2017.03.021.

Gao, X., Omosebi, A., Landon, J., Liu, K., 2015a. Surface charge enhanced carbon electrodes for stable and efficient capacitive deionization using inverted adsorption–desorption behavior. Energy Environ. Sci. 8, 897–909. http://dx.doi.org/10.1039/C4EE03172E.

Gao, X., Omosebi, A., Landon, J., Liu, K., 2015b. Enhanced salt removal in an inverted capacitive deionization cell using amine modified microporous carbon cathodes. Environ. Sci. Technol. 49, 10920–10926. http://dx.doi.org/10.1021/acs.est.5b02320.

Gao, X., Omosebi, A., Landon, J., Liu, K., 2014. Enhancement of charge efficiency for a capacitive deionization cell using carbon xerogel with modified potential of zero charge. Electrochem. Commun. 39, 22–25. http://dx.doi.org/10.1016/j.elecom.2013.12.004.

Gao, X., Porada, S., Omosebi, A., Liu, K.-L., Biesheuvel, P.M., Landon, J., 2016. Complementary surface charge for enhanced capacitive deionization. Water Res. 92, 275–282. http://dx.doi.org/10.1016/j.watres.2016.01.048.

He, D., Wong, C.E., Tang, W., Kovalsky, P., Waite, T.D., 2016. Faradaic reactions in water desalination by batch-mode capacitive deionization. Environ. Sci. Technol. Lett. http://dx.doi.org/10.1021/acs.estlett.6b00124 acs.estlett.6b00124.

Hemmatifar, A., Palko, J.W., Stadermann, M., Santiago, J.G., 2016. Energy breakdown in capacitive deionization. Water Res. 104, 303–311. http://dx.doi.org/10.1016/j.watres.2016.08.020.

Hemmatifar, A., Stadermann, M., Santiago, J.G., 2015. Two-dimensional porous electrode model for capacitive deionization. J. Phys. Chem. C 119, 24681–24694. http://dx.doi.org/10.1021/acs.jpcc.5b05847.

Johnson, A.M., Newman, J., 1971. Desalting by means of porous carbon electrodes. J. Electrochem. Soc. 118, 510. http://dx.doi.org/10.1149/1.2408094.

Kang, J., Kim, T., Jo, K., Yoon, J., 2014. Comparison of salt adsorption capacity and energy consumption between constant current and constant voltage operation in capacitive deionization. Desalination 352, 52–57. http://dx.doi.org/10.1016/

j.desal.2014.08.009.
Kim, T., Yoon, J., 2014. CDI ragone plot as a functional tool to evaluate desalination performance in capacitive deionization. RSC Adv. 5, 1456–1461. http://dx.doi.org/10.1039/C4RA11257A.
Lee, J.-H.H., Bae, W.-S.S., Choi, J.-H.H., 2010. Electrode reactions and adsorption/desorption performance related to the applied potential in a capacitive deionization process. Desalination 258, 159–163. http://dx.doi.org/10.1016/j.desal.2010.03.020.
Lopez-Ramon, M.V., Stoeckli, F., Moreno-Castilla, C., Carrasco-Marin, F., 1999. On the characterization of acidic and basic surface sites on carbons by various techniques. Carbon N. Y. 37, 1215–1221. http://dx.doi.org/10.1016/S0008-6223(98)00317-0.
Noh, J.S., Schwarz, J.A., 1990. Effect of HNO3 treatment on the surface acidity of activated carbons. Carbon, 28 (5), 675–682. http://dx.doi.org/10.1016/0008-6223(90)90069-B.
Pandolfo, A.G., Hollenkamp, A.F., 2006. Carbon properties and their role in supercapacitors. J. Power Sources 157, 11–27. http://dx.doi.org/10.1016/j.jpowsour.2006.02.065.
Persat, A., Chambers, R.D., Santiago, J.G., 2009a. Basic principles of electrolyte chemistry for microfluidic electrokinetics. Part I: acid-base equilibria and pH buffers. Lab. Chip 9, 2437–2453. http://dx.doi.org/10.1039/b906465f.
Persat, A., Suss, M.E., Santiago, J.G., 2009b. Basic principles of electrolyte chemistry for microfluidic electrokinetics. Part II: coupling between ion mobility, electrolysis, and acid-base equilibria. Lab. Chip 9, 2454–2469. http://dx.doi.org/10.1039/b906468k.
Porada, S., Zhao, R., van der Wal, A., Presser, V., Biesheuvel, P.M., 2013. Review on the science and technology of water desalination by capacitive deionization. Prog. Mater. Sci. 58, 1388–1442. http://dx.doi.org/10.1016/j.pmatsci.2013.03.005.
Qu, Y., Baumann, T.F., Santiago, J.G., Stadermann, M., 2015. Characterization of resistances of a capacitive deionization system. Environ. Sci. Technol. 1–15. http://dx.doi.org/10.1021/acs.est.5b02542.
Qu, Y., Campbell, P.G., Gu, L., Knipe, J.M., Dzenitis, E., Santiago, J.G., Stadermann, M., 2016. Energy consumption analysis of constant voltage and constant current operations in capacitive deionization. Desalination 400, 18–24. http://dx.doi.org/10.1016/j.desal.2016.09.014.
Suss, M., Porada, S., Sun, X., Biesheuvel, P.M., Yoon, J., Presser, V., 2015. Water desalination via capacitive deionization: what is it and what can we expect from it? Energy Environ. Sci. http://dx.doi.org/10.1039/C5EE00519A.
Wu, T., Wang, G., Zhan, F., Dong, Q., Ren, Q., Wang, J., Qiu, J., 2016. Surface-treated carbon electrodes with modified potential of zero charge for capacitive deionization. Water Res. 93, 30–37. http://dx.doi.org/10.1016/j.watres.2016.02.004.
Zhao, R., Biesheuvel, P.M., Miedema, H., Bruning, H., van der Wal, A., 2010. Charge efficiency: a functional tool to probe the double-layer structure inside of porous electrodes and application in the modeling of capacitive deionization. J. Phys. Chem. Lett. 1, 205–210. http://dx.doi.org/10.1021/jz900154h.